Theor Chem Acc (2012) 131:1154
DOI 10.1007/s00214-012-1154-6

REGULAR ARTICLE

Theoretical investigation of molecular excited states in polar organic monolayers via an efficient embedding approach

Aleksandrs Terentjevs · Eduardo Fabiano · Fabio Della Sala

Received: 28 June 2011 / Accepted: 13 September 2011 / Published online: 17 February 2012

Abstract In this work, we present a theoretical investigation on excitation energies of organic molecules embedded in a periodic monolayer. We use the self-consistent periodic-image-charges embedding approach, which takes into account all the electrostatic effects, to compute the perturbation on molecular orbitals and eigenvalues due to the presence of the surrounding periodic array of polar molecules. We considered vanadyl naphthalocyanine, mercaptobiphenyl, and tris-(8-hydroxyquinoline) aluminum (AlQ_3) at different coverages, and excitation energies computed using the time-dependent density-functional theory. We found a significant (0.1–0.2 eV) red- or blue-shift of the energies for different excited states, due to the different coupling of the molecule with the polarization field of the two-dimensional crystal.

Keywords Self-assembled monolayers · Time-dependent density-functional theory · QM/MM · Excited state · Polarizability · Workfunction shift

Dedicated to Professor Vincenzo Barone and published as part of the special collection of articles celebrating his 60th birthday.

A. Terentjevs · E. Fabiano · F. Della Sala (✉)
National Nanotechnology Laboratory (NNL),
Istituto Nanoscienze-CNR, Via per Arnesano 16,
73100 Lecce, Italy
e-mail: fabio.dellasala@unisalento.it

F. Della Sala
Center for Biomolecular Nanotechnologies @UNILE,
Istituto Italiano di Tecnologia (IIT), Via Barsanti,
73010 Arnesano, Italy

1 Introduction

Spontaneously assembled ordered single layers of polar organic molecules (SAMs) play an important role in many research areas [1–4]. In particular, they are largely employed in molecular (opto)electronics [5] to modify the effective work function of a surface and achieve a fine tuning of charge injection barriers and level alignment with additional organic adsorbates [6].

The work-function shift ($\Delta\Phi$) induced by a SAM of polar molecules is given (in atomic units) by the Helmholtz equation [7]

$$\Delta\Phi(n) = -4\pi n\mu_z(n) \tag{1}$$

where n is the number of molecules per unit area, μ_z is the z-component of the electronic molecular dipole, and we assumed the z-axis to be perpendicular to the surface. The molecular dipole can be further decomposed as $\mu_z(n) = \mu_z^{\mathrm{SAM}}(n) + \mu_z^{\mathrm{bond}}$ where μ_z^{SAM} is the z-component of the dipole moment of a molecule in the isolated SAM (i.e., without any substrate) and μ_z^{bond} is the so called bond-dipole [8–10]. The latter is determined by the interaction of the molecules with the surface and represents usually a rather small and local effect, quite independent on the structure of the SAM [8–10]. On the contrary, the dominating SAM's dipole depends strongly on the electronic properties of the molecules constituting the SAM and from the exact SAM's structure [7, 11].

Considering a SAM of polar molecules, in first approximation, as a two-dimensional (2D) infinite periodic array of point dipoles, μ_z^{SAM} is given by the Topping formula [12–14]

$$\mu_z^{\mathrm{SAM}}(n) = \frac{\mu_z^0}{1 + n^{3/2} f \alpha_{zz}} \tag{2}$$

with μ_z^0 the z-component of the dipole moment of the isolated molecule, α_{zz} the zz-component of the electric polarizability tensor, and f a numerical factor depending on the lattice periodic structure [12]. The Topping formula Eq. 2 provides an efficient qualitative tool to study depolarization effects in SAMs but, due to its approximations, suffers for several drawbacks, including the lack local-field and high-multipole effects, which are especially severe at high coverages [11].

An improved description of the problem is obtained performing full quantum simulations of the entire 2D system (see, e.g., Refs. [8–10]), using density-functional theory (DFT), with plane wave (PW) basis functions and periodic boundary conditions, within a supercell approach using a dipole-correction scheme [15]. Nevertheless, this approach has a high computational cost for low- and medium-coverage regimes [16] and, more importantly, is practically restricted to local or semilocal density functionals. This latter constrain implies several limitations in the description of the electronic structure of organic molecules [17–19], for example, the dipole moment and polarizability of conjugated systems [11, 20–22]. Alternative computational approaches, possibly including hybrid [23] and orbital-dependent treatments [24–26], are therefore desiderable.

Recently, we proposed an alternative approach to treat the depolarization in SAMs of polar organic molecules by introducing the self-consistent periodic-image-charges embedding (SPICE) method [11]. This is based on localized-orbitals quantum-mechanical calculations within a periodic-charge embedding scheme and allows to treat at any level of theory (including, e.g., coupled-cluster methods) the depolarization effect with good accuracy and high efficiency. In previous works [11, 22], the SPICE method was applied only to acquire information on the total ground-state density and the corresponding work-function shift. However, it is more general and can be applied also to excited states, similarly as other embedding methods [27]. In particular, it can be used to compute the perturbation within a SAM, due to the surrounding molecules, on the wavefunction and eigenvalues of different molecular orbitals and thus also modifications of the excitation energies (see Sect. 3).

In this paper, we consider this new aspect and we focus on the modifications of the excitation spectrum of molecular species when these are packed together to form a SAM extending infinitely in two dimensions. We will consider the case in which only a single molecule is excited, whereas all the other molecules are frozen in their ground state. Such a description is well suited to model optical experiments in molecular films and crystals in which the population of excited molecules is very low [28, 29]. In addition, as the lowest excited states of organic molecules are rather localized and we are interested in the low coverage regime, the electron-hopping probability among different molecules is small. In fact, we are not aiming to model the excitation energies of a molecular crystal or slab, whose excited states need to described in term of excitonic and/or charge-transfer bands [30–33]. Our approach is instead relevant to compute directly the polarization term of the excitonic band-structure [34, 35], to describe the excited-state depolarization in thin organic films [29], to study the dependence of single-molecule excited states on the coverage [36], and to describe the modifications of the photoluminescence of single molecule in a molecular crystal [34, 37].

To this end, we apply the SPICE method to study the depolarization effect and the single-molecule excitation spectrum in three typical SAMs with significant dipole moment and employed in molecular electronic and optoelectronic applications, namely those of vanadyl naphthalocyanine (VONc) [38], mercaptobiphenyl [39, 40], and tris-(8-hydroxyquinoline) aluminum (AlQ_3) [41] (for the latter both the facial and the meridional configurations were considered). The geometries and the unit cells of the all considered systems are reported in Fig. 1.

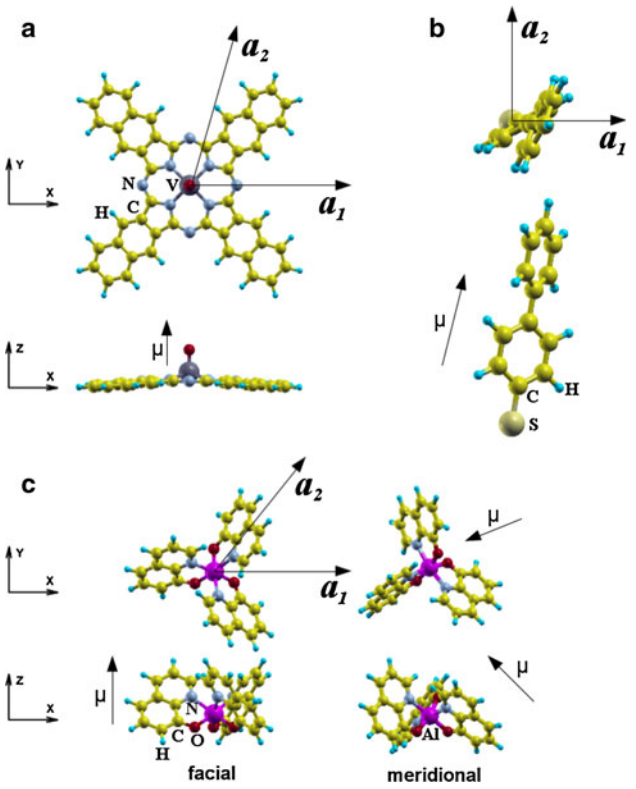

Fig. 1 Investigated systems: **a** VONc, **b** Biphenyl, **c** AlQ_3 facial and meridional. The dipole moment $\boldsymbol{\mu}$ and the lattice unit vectors $\mathbf{a}_1$ and $\mathbf{a}_2$ are also indicated

VONc has been largely investigated from an experimental point view [29, 36, 38, 42] due to its large dipole moment perpendicular to a large macrocyle; mercaptobiphenyl has been the subject of many theoretical studies as a model system of SAM/metal interfaces [10, 16, 39, 40]; AlQ_3 is a molecule often employed in the realization of optoelectronic devices [43–47].

2 Method

The ground-state electronic structure of a single, isolated molecule can be obtained, within the Kohn–Sham DFT or Hartree–Fock approach, solving

$$\hat{H}^0[\rho^0]\phi_i^0(\mathbf{r}) = \epsilon_i^0\phi_i^0(\mathbf{r}), \tag{3}$$

where H^0 is the Hamiltonian of a single isolated molecule, $\rho^0(\mathbf{r}) = \sum_{i=1}^{N/2} |\phi_i^0(\mathbf{r})|^2$ is the electron density (for simplicity we consider a closed-shell system with $N/2$ occupied orbitals), $\{\phi_i^0\}$ are the Kohn–Sham orbitals, and the superscript ^{0} denotes the ground-state unperturbed (isolated) quantities. The Hamiltonian contains the kinetic, the external potential, and the Coulomb-exchange-correlation operator. Therefore, it depends on ρ^0 (thus on $\{\phi_i^0\}$), requiring a self-consistent solution of Eq. 3.

To include the perturbation due to the 2D monolayer, we consider the perturbed Hamiltonian of a single unit cell (for simplicity we consider the case of one molecule per unit cell)

$$\hat{H}[\rho] = \hat{H}^0[\rho] + V_{\text{emb}}[\rho](\mathbf{r}), \tag{4}$$

where ρ is now the perturbed molecular density, $H^0[\rho]$ is the Hamiltonian of a single isolated molecule but computed at the perturbed density, and V_{emb} is the embedding potential including the interaction of the molecule with the rest of the monolayer. The perturbed molecular orbitals (ϕ_i) and eigenvalues (ϵ_i) are then obtained from the equation

$$\hat{H}[\rho]\phi_i(\mathbf{r}) = \epsilon_i\phi_i(\mathbf{r}), \tag{5}$$

with $\rho(\mathbf{r}) = \sum_{i=1}^{N/2} |\phi_i(\mathbf{r})|^2$.

Within the SPICE method, the embedding potential V_{emb} is restricted to a Coulomb interaction and is given by

$$V_{\text{emb}}[\rho](\mathbf{r}) = \sum_{(i,j)\neq(0,0)} \int d\mathbf{r}' \frac{q(\mathbf{r}' - i\mathbf{a_1} - j\mathbf{a_2})}{|\mathbf{r} - \mathbf{r}'|}, \tag{6}$$

with q the sum of the (fixed) nuclear and electronic charge densities. Equation 6 represents the electrostatic potential on the central molecule (i.e., with $i = j = 0$) due to all the surrounding molecules in the monolayer. It can be computed efficiently, introducing only a small overhead with respect to a single-molecule calculation, through the fast multipole method [48] after an expansion of q in localized charges (e.g., Mulliken charges). The embedding potential can be also generalized to include kinetic-exchange-correlation effects [49, 50], but these introduce additional computational complications and are only relevant for the high coverage regime. The coverage dependence is implicitly included in Eq. 6 through the lattice vectors $\mathbf{a}_1$ and $\mathbf{a}_2$.

Equations 4, 5, and 6 define the SPICE method and are solved in a double self-consistent loop requiring typically 3–5 steps for convergence.

It is worth to underline that (i) in the SPICE method, the full periodic structure of the monolayer is taken into account, and thus, it is different from other approaches that employ a finite cluster of molecules to model the environment [28, 51, 52] and are limited by the slow convergence of the electronic properties with system size; (ii) the SPICE method does not need any external parametrization, as it is required instead to model the QM/MM interaction with a solvent, nor the computation of the atom–atom polarizabilities [53] because the QM molecule is interacting with *images* of itself, which are computed at the same QM level of theory, and thus with the exact QM density and polarization.

The perturbed molecular orbitals (ϕ_i) and eigenvalues (ϵ_i) resulting from the solution of Eq. 5 differ from the ones of the isolated molecule (ϕ_i^0, ϵ_i^0) due to the electrostatic interaction with the surrounding molecules. They can be used to evaluate the ground-state electronic properties of the monolayer directly or through their use in post-Hartree–Fock wavefunction methods (e.g., CC2). In addition, excitation energies can then be evaluated via the linear response time-dependent DFT (TD-DFT) [54] formalism, using the perturbed orbitals and eigenvalues, or applying correlated wavefunction methods.

Note that in the present approach, no response of the environment to the excitation is included in the TD-DFT kernel. Therefore, we only model single-molecule excitations in a static embedding environment (analogous with static solvation models or biological environment). However, as discussed in the introduction, we are not aiming at describing excitonic splittings and long-range dielectric effects are expected to be quite small in a thin monolayer. Nevertheless, dynamic embedding effects can be possibly incorporated by considering the TD-DFT extension of the FDE theory [55–57].

3 Computational details

For all molecules, the gas-phase equilibrium geometry optimized at the APBE/def2-TZVP [58–60] level was considered. This is expected to be a fair choice for the

relatively low coverages studied in this work. The APBE functional was chosen because of its ability to yield reasonably accurate geometries for both conjugated and metal-organic molecules [58].

The VONc monolayer was constructed considering high-resolution STM studies of Fe-phthalocyanine on an Au (111) surface [61], using a monoclinic cell with an angle of 81.8° between the primitive vectors (see Fig. 1a) and lattice constants varying from 18 Å (full coverage) to 53 Å. The use of experimental data referring to a Fe-phthalocyanine SAM was motivated by the lack of information in literature about the structure of SAMs of VONc molecules. This choice is expected anyway to have a negligible impact on the results of the present study.

For mercaptobiphenyl, a simple square cell was considered (see Fig. 1b). The molecule was assumed to be tilted with respect to the 2D plane by 10°, in agreement with PW-DFT calculations [40]. The cell-side dimensions were varied from 7.4 to 53 Å.

Finally, for both AlQ_3 configurations, we considered a monoclinic cell with an angle of 60° between the lattice vectors (see Fig. 1c). This was deduced from previous theoretical works considering the absorption of AlQ_3 on an aluminum (111) surface [41]. The dimensions of the cell were ranging from 11.6 to 53 Å.

All calculations were performed using the TURBOMOLE program package [62]. The APBE [58], BLYP [63, 64], B3LYP [23, 64], BHLYP [65], and PBE0 [66] functionals were considered, and the def2-TZVP basis set [59, 60] was used in all cases. In addition, approximate single and double coupled-cluster (CC2) [67, 68] calculations were performed for benchmark purposes using the cc-pVTZ [69] basis set.

4 Results

4.1 VONc

In this molecule, a large dipole moment is present due to the V–O group (see Fig. 1a). In Fig. 2, we report the work-function shift (computed with the SPICE method using Eq. 1) as a function of the VONc coverage and compare it with experimental data for VONc on highly oriented pyrolytic graphite [38].

The computed data agree well with experimental ones up to a coverage of 0.6 monolayers (ML) for all methods considered. The workfunction shift increases with the fraction of exact exchange in the series BLYP, B3LYP, BHLYP. APBE (not shown) almost coincides with BLYP. The increase of the work-function shift is directly related to the increase of the module of the V–O dipole moment that is 0.99 a.u., 1.05 a.u., and 1.15 a.u. at the BYLP, B3LYP, and BHLYP level, respectively. The comparison between the theoretical and experimental results seems to indicate, surprisingly, a better agreement for the BLYP functional. However, two main issues need to be considered: (i) The experimental data are expressed as a function of the monolayer (ML) fraction, while the theoretical results are obtained as a function of the number of molecules per unit surface. Since no information is available about the exact molecular density at 1 ML experimental conditions, the comparison is necessarily approximate. In plotting Fig. 2, we assumed for the full coverage limit a unit cell with a size of 18 Å. This is, however, a lower limit for the cell dimension, dictated by the steric repulsion between neighboring molecules, while the true cell dimension might be expected to be slightly larger. Increasing slightly the minimum cell dimension (i.e., expanding the x-axis of Fig. 2 for the theoretical data) causes the experimental curve to approach more the BHLYP one, thus making hybrid functionals in better agreement with the experiment. We recall in addition that in the present work, the monolayer was constructed using the experimental data for Fe-phthalocyanine rather than VONc. While this is not a problem at low coverages, where the exact structure of the SAM plays a minor role, it can lead to some small discrepancies at particularly high coverages where, due to different inter-molecular interactions, the arrangement of the molecules in the SAM might be different also for similar species.

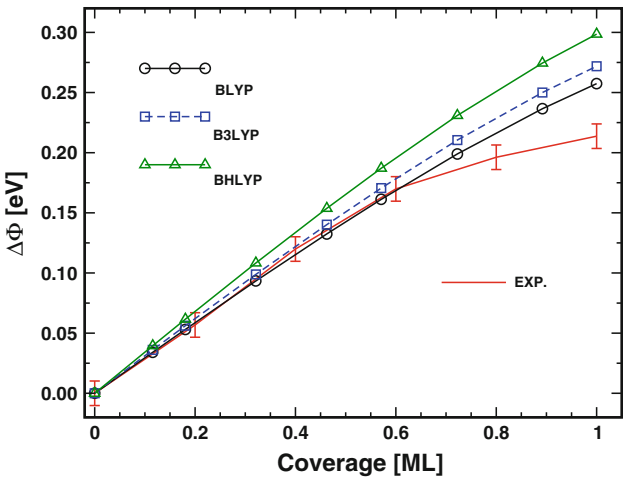

Fig. 2 Work-function shift for the VONc monolayer as a function of coverage, from SPICE calculations with different exchange-correlation functionals. Experimental data are taken from Ref. [38]

(ii) The experimental measurements were performed for VONc on a pyrolytic graphite surface, while simulations considered an isolated monolayer. Although the interaction of VONc with the graphite surface is small (certainly much smaller than, e.g., with metal substrates), an interfacial bond-dipole (μ^{bond}) cannot be excluded [70]. The latter,

being in opposite direction to the V–O dipole, will reduce the computed work-function shift, making again BHLYP in better agreement with experiment.

At higher coverage, on the other hand, all functionals overestimate the experimental results, which show a clear reduction of the steepness of the curve. In addition to the above two points, we cannot rule out that other effects (e.g., kinetic-exchange-correlation) play a relevant role at the highest coverage, because these effects are not included in SPICE simulations. Moreover, at short intramolecular distances, the expansion of the molecular electron density in localized Mulliken charges is inappropriate to represent correctly the high-multipole moments and the strong local-field effects that contribute at these coverages. Despite all the above considerations, Fig. 2 clearly shows that up to 0.8 ML the SPICE method can describe very well the electronic properties of the VONc monolayer.

Concerning the variation of the excitation energy with the coverage (not reported), it is found to be negligible (smaller than 0.01 eV). This traces back to the fact that the VONc has its aromatic π system perpendicular to the molecular dipole and the latter is well localized on the V–O bond. Thus, the electrostatic field produced by the molecules in the monolayer is small and roughly uniform in the plane of the molecule. In fact, we found that all molecular orbitals display a similar shift in energy, and thus, the energy-gap and the excitation energies are not modified with the coverage: for example, the HOMO shifts by 0.17 eV (from isolated molecule to the coverage 0.9 ML) while LUMO shifts by 0.18 eV giving, an energy-gap difference of only 0.01 eV.

4.2 Mercaptobiphenyl

Larger shifts in excitation energies can be obtained when the dipole is parallel to the highly polarizable π-electron system: this is the case for mercaptobiphenyl. In this molecule, the depolarization is caused by the interaction of the dipole localized on the thiol group with the polarizable π-conjugated molecular backbone (see Fig. 1b). Because the dipole moment is directed in the same direction as the conjugated molecular backbone, and the π-electron density is highly polarizable in this direction, the depolarization is particularly relevant for this system and significantly larger than for the VONc molecule, where the dipole moment is pointing perpendicular to the π-plane.

Previous studies showed that an accurate description of the work-function shift can be achieved using hybrid or orbital-dependent functionals (see Fig. 2 of Ref. [11] and Fig. 4 of Ref. [22]). Local and semilocal functionals give instead a significant overestimation of both the dipole moment and the polarizability [22]. As a consequence, they yield a poor description of the depolarization at low- and medium-coverage, while they rely on an error cancelation at the highest coverages [11, 22].

In this paper, we use the mercaptobiphenyl as a model system to study the coverage dependence of singlet excitations in self-assembled monolayer. In Fig. 3, we report the lowest singlet excitations energies as a function of the number of molecules per unit area in the monolayer (the S_1 state lays much lower in energy and it shows the same behavior as the S_2 and S_3 states: it is not reported to keep the readability of Fig. 3). The calculations were performed at the PBE0 level, because this functional provides a good description of the depolarization effect and it includes nonlocality in the kernel.

Inspection of Fig. 3 shows that different excitations display different behaviors with the coverage. In particular, the lowest excited states show increasing energies with increasing coverage. On the contrary, the two highest singlets display a decrease of the excitation energy as the coverage increases. Interestingly, it is also possible to have different slopes for the lines so that two excited states can cross. This is the case of the S_4 (dark) and S_5 (with the highest oscillator strength) excited states that display an avoided crossing at a molecular density of about 0.004 Bohr^{-2}. This finding can open a new route in the design of optoelectronic devices. In fact, it can allow, for example, to control the radiative/nonradiative decay rates of the molecule inside the monolayer, as a function of the coverage.

To rationalize these results, it is useful to keep in mind the single-particle character of the excitations and look closer to the coverage dependence of the energies of the molecular orbitals involved in these excitations. They are

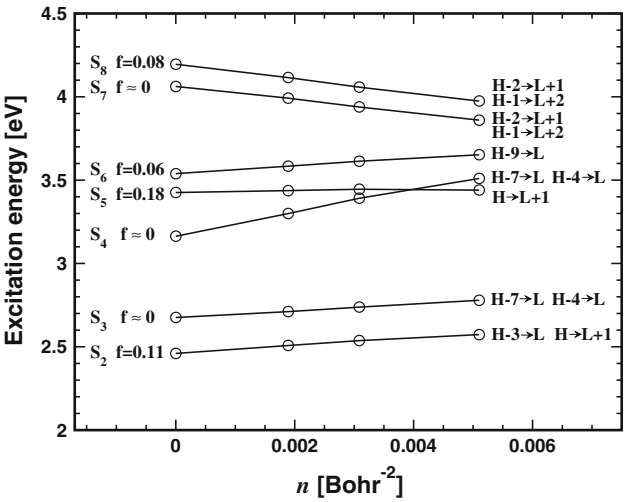

Fig. 3 TD-PBE0 singlet excitation energies of the mercaptobiphenyl as functions of the monolayer molecular density. The oscillator strength f of each state is also reported. S_1 (not shown) has a very low energy and $f \approx 0$. The single-particle character of the excitations is indicated on the right side (H HOMO, L LUMO)

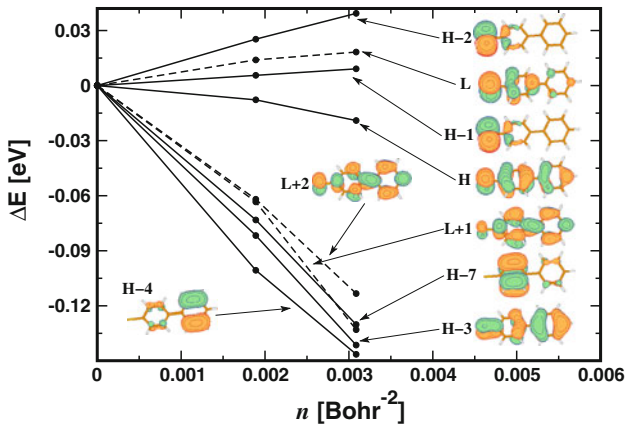

Fig. 4 Orbital energies (*H* HOMO, *L* LUMO) as a function of the molecular density for mercaptobiphenyl. Virtual orbitals are denoted with *dashed lines*

reported in Fig. 4. Orbitals with a significant localization on the thiol group (e.g., HOMO-2) increase their energy with increasing coverage, while those which are mainly localized on the biphenyl (e.g., H-4) lower their energy when the coverage increases. Thus, excitations that cause an increase of electron density on the thiol part and/or a reduction on the biphenyl (e.g., S_2) will increase their energy with increasing coverage, while the opposite will happen for excitations increasing the electron density on the molecular backbone and/or reducing it on the sulfur (e.g., S_7). A simple rationalization of the trend observed for the orbital energies is given by the observation that the field produced by the molecular dipole moments in the monolayer leads to a depolarization; hence, it tends to remove electron charge from the sulfur atom and to place it on the biphenyl. Therefore, the orbitals with some localization on the sulfur are increasingly destabilized when the coverage (i.e., the dipolar field) increases. For the same reason, the orbitals localized on the biphenyl are stabilized at higher coverages.

4.3 AlQ_3

The AlQ_3 molecule is an interesting case study in the present work because of its very high dipole moment in a different orientation than the previous two systems. This dipole originates mainly from the charge polarization around the central Al atom, due to the different electron affinities of the nitrogen and oxygen atoms interacting with the central metal (see Fig. 1c). AlQ_3 presents two main isomers, the meridional-AlQ_3 (mer-AlQ_3) and the facial-AlQ_3 (fac-AlQ_3), which differ for the position of oxygen and nitrogen atoms around the central metal Al atom. In fac-AlQ_3 in the central distorted octahedral coordinated site each oxygen atom faces a nitrogen so that three polarized O-Al-N linear bonds are formed, while in mer-AlQ_3 only one O-Al-N linear bond is observed and the dipole moment of fac-AlQ_3 is significantly larger than the one of mer-AlQ_3. Moreover, since for fac-AlQ_3, the molecular dipole moment is oriented perpendicular to the monolayer plane, while for mer-AlQ_3 it is tilted, very large differences in the magnitude of μ_z are observed. Both isomers present instead a very similar polarizability, thus a similar depolarization effect can be expected.

In the upper part of Fig. 5, we report the dipole moments of fac-AlQ_3 and mer-AlQ_3 as a function of the molecular density, calculated with the GGA PBE functional and the hybrid PBE0 functional. CC2 results are also shown for reference. For both isomers, a similar trend with the molecular density is found, as expected. The depolarization effect is described also rather similarly by both DFT methods. This relates well with the fact that the computed *zz*-polarizability are similar: 345.6 a.u. (366.9 a.u.) and 337.1 a.u. (358.0 a.u.) from PBE and PBE0, for fac-AlQ_3(mer-AlQ_3). Larger differences are found instead between PBE and PBE0 for what concerns the absolute value of the dipole moment. For the isolated fac-AlQ_3, PBE0 yields $\mu_z = 3.01$ a.u. while PBE gives a dipole moment of 2.74 a.u.. Similarly, for the mer-AlQ_3, dipole moments of 1.10 and 1.01 a.u. are obtained with PBE0 and PBE, respectively. A comparison with the CC2 calculations ($\mu_z = 2.90$ a.u. for fac-AlQ_3 and $\mu_z = 1.06$ a.u. for mer-AlQ_3) indicates that relatively accurate results are produced by DFT calculations employing the hybrid PBE0 functional, despite the polarizability (hence the depolarization) is overestimated at this level of theory. Poorer results are found with the PBE GGA functional, which yields a clear underestimation of the dipole moment.

Turning to excitation energies, we note preliminarily that a reasonably good description of the lowest singlet excited states can be obtained from TD-DFT calculations using the PBE0 functional. The calculations yield in fact a lower absorption band around 3 eV and a second band between 4 and 5 eV (not shown). These results compare well with those obtained in optical absorption measurements on amorphous AlQ_3 thin films (see Fig. 5 of Ref. [71]), except for a small underestimation of the excitation energies.

The evolution of excitation energies with the molecular density in the monolayer was simulated with the SPICE method at the TD-PBE0 level. Inspection of the bottom panels of Fig. 5 reveals two distinct behaviors. For fac-AlQ_3. all the examined excited states show decreasing energy with increasing coverage. For mer-AlQ_3, on the other hand, some excitation energies (S_1, S_4, S_5, S_6) increase with the coverage, while some of them (S_2, S_3, S_7, S_8, S_9) decrease. This makes the mer-AlQ_3 more interesting from the photophysical point of view because it offers the possibility of tuning the device performance through a

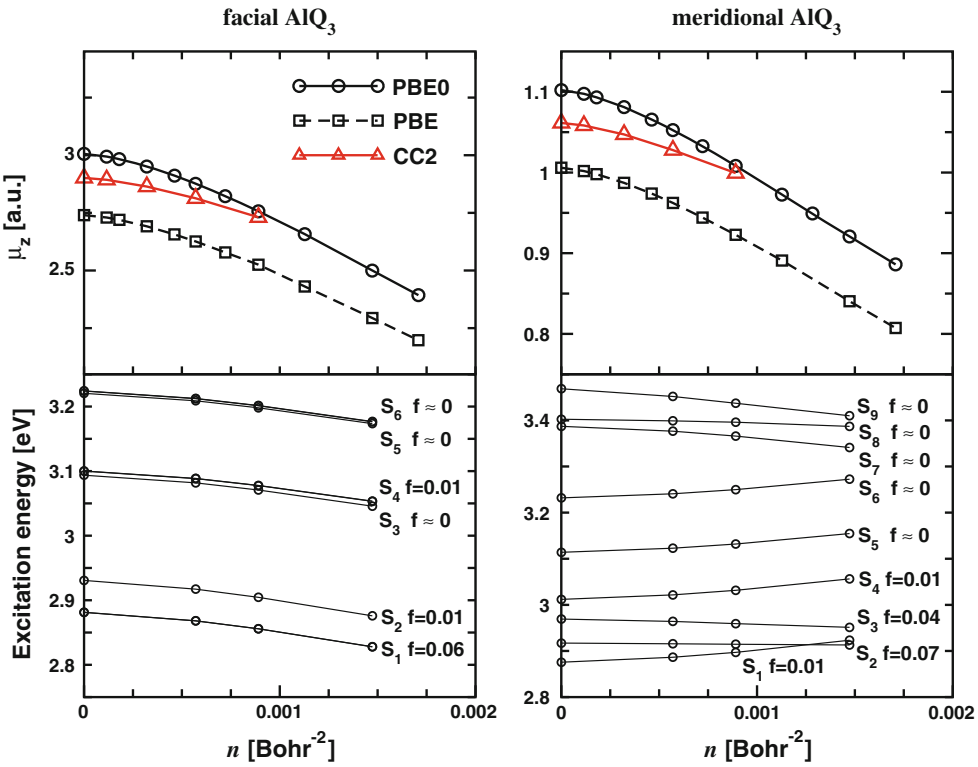

Fig. 5 Dipole moments (*top*) and excitation energies (*bottom*) of fac-AlQ_3 and mer-AlQ_3 as a function of the molecular density. Excitation energies were computed at the TD-PBE0 level of theory

modification of the excited-state energy gaps by varying the coverage. On the other hand, fac-AlQ_3 retains the isolated molecule properties.

The behavior of the different excitation energies can be rationalized in a similar way as for the biphenyl case, although here a more complex situation is faced due to the complicated structure of the AlQ_3 molecule. In general, molecular orbitals that present a stronger localization are more destabilized at high coverages than those that are rather delocalized. The latter can in fact relax more easily to respond to the external perturbation induced by the interaction in the monolayer.

5 Conclusions

The SPICE method is an efficient and powerful tool to perform theoretical investigations on periodic organic monolayers at low- and medium-coverages. It was in fact already successfully employed to study the depolarization effect and work-function shift in several systems as well as to assess the limitations of conventional DFT approaches [11].

In this work, the SPICE method has been extended to the calculation of the coverage dependence of excited states: single-molecule excitation spectra of VONc, mercaptobiphenyl, and AlQ_3 monolayers at different coverages were investigated.

We found that for molecules possessing a large dipole perpendicular to the monolayer plane and low-lying excitations characterized by single-particle transitions between orbitals with different characters (e.g., $n \rightarrow \pi^*$ transitions), large variations in the excitations energies are observed. This is the case for the example of mercaptobiphenyl and AlQ_3. The evolution of the excitation energies with the coverage was rationalized in terms of the increased stability of molecular orbitals with a large polarizability in the direction of the monolayer dipole. The opposite occurs for orbitals that cannot properly respond to the monolayer perturbing field, as in the case of rather localized orbitals.

The possibility of tuning the excitation-energy gaps by varying the coverage opens new ways to design and engineer molecular (opto)electronic devices with higher efficiency. The present work brings a fundamental contribution in this context by providing a rationale for the basic understanding of the phenomenon at the molecular level. Moreover, it proposes the SPICE method as an efficient tool for the simulation of single-molecule excitations in organic monolayers.

Acknowledgments We thank TURBOMOLE GmbH for providing us with the TURBOMOLE program package, and M. Margarito for technical support. This work was funded by the European Research Council (ERC) Starting Grant FP7 Project DEDOM, Grant Agreement No. 207441.

References

1. Ulman A (1996) Chem Rev 96:1533
2. Arima V, Fabiano E, Blyth RIR, Della Sala F, Matino F, Thompson J, Cingolani R, Rinaldi R (2004) J Am Chem Soc 126:16951
3. Love JC, Estroff LA, Kriebel JK, Nuzzo RG, Whitesides GM (2005) Chem Rev 105:1103
4. Heimel G, Romaner L, Zojer E, Brédas JL (2008) Acc. Chem. Res. 41:721
5. Tao N (2006) Nat Nanotech 1:173
6. Sushko ML, Shluger AL (2009) Adv Mater 21:1111
7. Romaner L, Heimel G, Ambrosch-Draxl C, Zojer E (2008) Adv Funct Mater 18:3999
8. Rusu PC, Brocks G (2006) J Phys Chem B 110:22628
9. Rusu PC, Brocks G (2006) Phys Rev B 74:073414
10. Heimel G, Romaner L, Zojer E, Brédas JL (2006) NanoLetters 7:932
11. Piacenza M, D'Agostino S, Fabiano E, Della Sala F (2009) Phys Rev B 80:153101
12. Topping J (1927) Proc R Soc Lond Ser A 114:67
13. Bagchi A, Barrera RG, Fuchs R (1982) Phys Rev B 25:7086
14. Maschhoff BL, Cowin JP (1994) J Chem Phys 101:8138
15. Bengtsson L (1999) Phys Rev B 59:12301
16. Romaner L, Heimel G, Zojer E (2008) Phys Rev B 77:045113
17. Johnson ER, Mori-Sánchez P, Cohen AJ, Yang W (2008) J Chem Phys 129:204112
18. Fabiano E, Della Sala F (2007) J Chem Phys 126:214102
19. Reimers JR, Cai ZL, Bili A, Hush NS (2003) Ann N Y Acad Sci 1006:235
20. Fuentealba P, Simn-Manso Y (1997) J Phys Chem A 101:4231
21. Kümmel S, Kronik L, Perdew JP (2004) Phys Rev Lett 93:213002
22. Della Sala F, Fabiano E, Laricchia S, D'Agostino S, Piacenza M (2010) Int J Quant Chem 110:2162
23. Becke AD (1993) J Chem Phys 98:5648
24. Della Sala F, Görling A (2001) J Chem Phys 115:5718
25. Kümmel S, Kronik L (2008) Rev Mod Phys 80:3
26. Della Sala F (2010) In: Springborg M (eds) Chemical modelling: applications and theory, vol 7, Royal Society of Chemistry, Cambridge, pp 115–161
27. Khait YG, Hoffmann MR (2010) J Chem Phys 133:044107
28. Kamiński R, Schmøkel MS, Coppens P (2010) J Phys Chem Lett 1:2349
29. Steele MP, Blumenfeld ML, Monti OLA (2010) J Phys Chem Lett 1:2011
30. Sariciftci, NS (eds) (1997) Primary photoexcitations in conjugated polymers: molecular exciton versus semiconductor band model. World Scientific, Singapore
31. Silbey R (1976) Ann Rev Phys Chem 27:203
32. Gigli G, Della Sala F, Lomascolo M, Anni M, Barbarella G, Di Carlo A, Lugli P, Cingolani R (2001) Phys Rev Lett 86:167
33. Yamagata H, Norton J, Hontz E, Olivier Y, Beljonne D, Brédas JL, Silbey RJ, Spano FC (2011) J Chem Phys 134:204703
34. Davidov A (1971) Theory of molecular excitons. Plenum Press, London
35. Müller M, Le Moal E, Scholz R, Sokolowski M (2011) Phys Rev B 83:241203
36. Steele MP, Blumenfeld ML, Monti OLA (2010) J Chem Phys 133:124701
37. Hochstrasser RM (1962) Rev Mod Phys 34:531
38. Blumenfeld ML, Steele MP, Monti OLA (2010) J Phys Chem Lett 1:145
39. Heimel G, Romaner L, Brédas JL, Zojer E (2006) Phys Rev Lett 96:196806
40. Fabiano E, Piacenza M, D'Agostino S, Della Sala F (2009) J Chem Phys 131:234101
41. Yanagisawa S, Lee K, Morikawa Y (2008) J Chem Phys 128:244704
42. Monti OLA, Steele MP (2010) Phys Chem Chem Phys 12:12390
43. Sirringhaus H, Tessler N, Friend RH (1998) Science 12:1741
44. Granström M, Petritsch K, Arias AC, Lux A, Andersson MR, Friend RH (1998) Nature 395:257
45. Gustafsson G, Cao Y, Treacy GM, Klavetter F, Colaneri N, Heeger AJ (1992) Nature 357:477
46. Friend RH, Gymer RW, Holmes AB, Burroughes JH, Marks RN, Taliani C, Bradley DDC, Santos DAD, Brdas JL, Lögdlund M, Salaneck WR (1999) Nature 397:121
47. Voss D (2000) Nature 407:442
48. Burow AM, Sierka M, Döbler J, Sauer J (2009) J Chem Phys 130:174710
49. Cortona P (1991) Phys Rev B 44:8454
50. Laricchia S, Fabiano E, Della Sala F (2010) J Chem Phys 133:164111
51. Cornil D, Olivier Y, Geskin V, Cornil J (2007) Adv Func Mater 17:1143
52. Norton JE, Brédas JL (2008) J Am Chem Soc 130:12377
53. Tsiper EV, Soos ZG (2001) Phys Rev B 64:195124
54. Casida ME (1995) Recent advances in density functional methods, vol 1. World Scientific, Singapore
55. Neugebauer J (2010) Phys Rep 489:1
56. Neugebauer J (2007) J Chem Phys 126:134116
57. Casida ME, Wesolowski TA (2004) Int J Quant Chem 96:577
58. Constantin LA, Fabiano E, Laricchia S, Della Sala F (2011) Phys Rev Lett 106:186406
59. Weigend F, Furche F, Ahlrichs R (2003) J Chem Phys 119:12753
60. Weigned F, Ahlrichs R (2005) Phys Chem Chem Phys 7:3297
61. Cheng ZH, Gao L, Deng ZT, Jiang N, Liu Q, Shi DX, Du SX, Guo HM, Gao HJ (2007) J Phys Chem C 111:9240
62. TURBOMOLE V6.1 2009: a development of University of Karlsruhe and Forschungszentrum Karlsruhe GmbH, 1989–2007, TURBOMOLE GmbH, since 2007; available from http://www.turbomole.com
63. Becke AD (1988) Phys Rev A 38:3098
64. Lee C, Yang W, Parr RG (1988) Phys Rev B 37:785
65. Becke AD (1993) J Chem Phys 98:1372
66. Adamo C, Barone V (1999) J Chem Phys 110:6158
67. Hättig C, Weigend F (2000) J Chem Phys 113:5154
68. Köhn A, Hättig C (2003) J Chem Phys 119:5021
69. Dunning TH Jr (1989) J Chem Phys 90:1008
70. Terentjevs A, Steele MP, Blumfeld ML, Ilyas N, Kelly LL, Fabiano E, Monti OLA, Della Sala F (2011) J Phys Chem C 115:21128
71. Brinkmann M, Gadret G, Muccini M, Taliani M, Masciocchi N, Sironi A (2000) J Am Chem Soc 122:5147